

A universal relation in NC-AFM, STM, and atom manipulation

C Julian Chen

Institute of Applied Physics and Microstructure Research Center, Hamburg University,
Jungiusstrasse 11, 20355 Hamburg, Germany

E-mail: jchen@physnet.uni-hamburg.de

Received 1 October 2004, in final form 26 November 2004

Published 11 January 2005

Online at stacks.iop.org/Nano/16/S27

Abstract

The imaging mechanism for both NC-AFM and STM at atomic resolution can be considered as a process of making and breaking of chemical bonds between the tip and the sample. Based on that concept, a universal relation between tunnelling conductance G and attractive atomic force F is established, which can be verified experimentally. This further implies an experimentally verifiable relation between the threshold resistance R and diffusion activation energy E in atom manipulation.

1. Introduction

It is now clear that the atomic resolution of non-contact AFM, for example on Si(111)7 × 7 [1], is due to the interaction between the sp³ dangling bond on the tip apex and the sp³ dangling bonds on the sample surface [2]. The imaging process is a sequence of making and breaking of partial chemical bonds between those dangling bond states. For STM, even in the early years, there was speculation that the observed atomic resolution on Si(111)7 × 7 was due to the interaction of the d_{z²} state on the W tip and the sp³ dangling bonds on the sample surface [3]. Meanwhile, early first-principles computation on STM showed that the tunnelling current of a W tip comes almost exclusively from various 5d states on the tip apex [4]. Quantitative analysis showed that such tip states were the origin of atomic resolution on metal surfaces with STM, as well as the origin of corrugation reversal observed on metal surfaces [5]. Consequently, the imaging mechanism of STM at atomic resolution is also a process of making and breaking of partial chemical bonds between the electronic states on the tip and the sample. In the last ten years, a number of first-principle computations have firmly established that on the apex of metal STM tips, various d states dominate the tip DOS, from 1 eV below the Fermi level up to 1 eV above the Fermi level [6–9]. The s states account for only a few per cent of the Fermi-level tip DOS, thus are insignificant. First-principle computations of STM images on metal surfaces have shown that the effect of d_{z²} states on the tip apex does enhance the corrugation of STM images by more than one order of magnitude, which adequately explains the observed atomic corrugations on metal surfaces [10, 11]. Therefore, the imaging mechanism of both

NC-AFM and STM at atomic resolution can be considered as a sequence of making and breaking of partial chemical bonds between the tip and the sample. From this point of view, at atomic resolution, both NC-AFM and STM are probing the basic building element of all condensed matter: the chemical bond.

There are fundamental similarities between the chemical bond and atom-scale tunnelling. Both are based on the overlap of wavefunctions of participating parties. Both are effective in the same distance range, a fraction of a nanometre. Both have an exponential dependence on the distance between the participating parties. In fact, the mathematical expression of the overlap integrals for the chemical bond and for tunnelling are identical. The mathematical expression for the prototype chemical bond energy, the hydrogen molecule ion, was discovered independently by Landau [12] and Herring [13] in the same year (1961). Almost at the same time, the mathematical expression of the tunnelling matrix element was discovered by Bardeen in 1960 [14]. It is worth noting that the dimension of Bardeen's tunnelling matrix element is *energy*, and it is mathematically identical to the interaction energy of the prototype chemical bond according to Landau and Herring.

The mathematical equivalence of the chemical bond energy and the tunnelling matrix element is not accidental. The origin of both can be traced to the concept of resonance in quantum mechanics, introduced by Heisenberg in 1926 [15]. Heisenberg's idea was applied by Pauling to become the basis of his theory of the chemical bond, the foundation of quantum chemistry [16]. In recent decades, because of the advance of computers and the development of density functional theory of quantum mechanics, the concept of resonance in

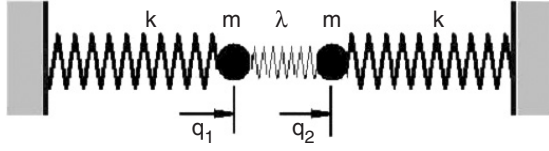


Figure 1. Concept of resonance, after Heisenberg.

quantum chemistry, especially for the computation of the ground states of molecules, is no longer essential. However, for NC-AFM and STM, because of the huge number of possible relative configurations of the tip *and* the sample, the intrinsic complexity of both, and the existence of well defined unperturbed original states—the free sample and the free tip, the theory of resonance, or the perturbation theory, is probably the most convenient formalism for its understanding.

Based on the similarity of the chemical bond and the tunnelling matrix element, an experimentally verifiable consequence between NC-AFM and STM, as well between the threshold resistance and diffusion activation energy in atom manipulation, can be established. In this paper, we provide a conceptual account of the theory, together with some suggested experiments.

2. Concept of resonance: Heisenberg

Right after his invention of quantum mechanics, Heisenberg published a paper entitled ‘Many-body problem and resonance in quantum mechanics’ [15]. His argument is as follows. In quantum mechanics, only a handful of one-particle problems can be solved analytically. For most practical systems, approximations are necessary. If a system is comprised of two separated systems, with a weak interaction between them, then the combined system can be resolved by treating the interaction as a resonance. To illustrate the concept and applications of resonance, Heisenberg provided an example in classical mechanics. Here it is.

The simplest example is a coupled harmonic oscillator with the Hamiltonian

$$H = \frac{1}{2m} p_1^2 + \frac{m}{2} \omega^2 q_1^2 + \frac{1}{2m} p_2^2 + \frac{m}{2} \omega^2 q_2^2 - 2\lambda m \omega q_1 q_2; \quad (1)$$

which is a pair of identical oscillators coupled by an interaction term, λ . Here, q_1 and q_2 are coordinates, p_1 and p_2 are momenta, m is the mass, and ω is the circular frequency of the individual oscillators. The Heisenberg Hamiltonian can be incarnated by a system of two masses and three springs, as shown in figure 1:

The relation between the spring constant k and the resonance frequency ω of the individual oscillators is

$$k = m\omega^2 - 2m\omega\lambda. \quad (2)$$

By holding one of the two masses still, the other mass would oscillate with angular frequency ω . The solutions are

$$q_1 = a_1 \cos(\omega t + \phi_1), \quad (3)$$

and

$$q_2 = a_2 \cos(\omega t + \phi_2), \quad (4)$$

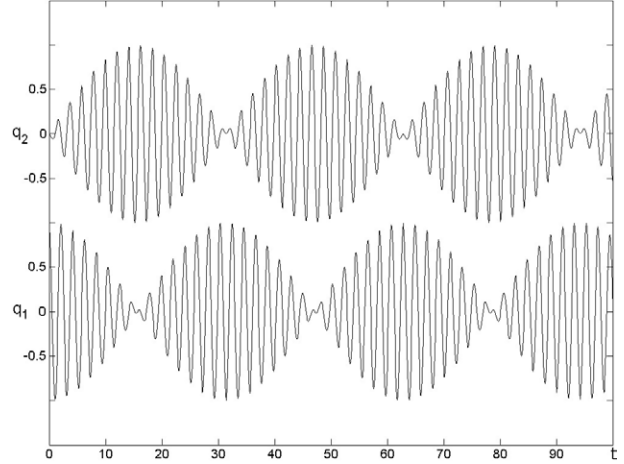


Figure 2. Time evolution of the coupled oscillator, showing resonance.

where a_1 and a_2 are amplitudes, and ϕ_1 and ϕ_2 are phases, respectively.

To facilitate the solution of the coupled system, we introduce two parameters (the approximate values are valid when $\lambda \ll \omega$),

$$\Omega = \frac{1}{2} \left[\sqrt{\omega^2 + 2\omega\lambda} + \sqrt{\omega^2 - 2\omega\lambda} \right] \cong \omega, \quad (5)$$

and

$$\Lambda = \frac{1}{2} \left[\sqrt{\omega^2 + 2\omega\lambda} - \sqrt{\omega^2 - 2\omega\lambda} \right] \cong \lambda. \quad (6)$$

Suppose at $t = 0$, $q_1 = a$ and $q_2 = 0$. The solutions of the coupled system are

$$q_1 = a \cos \Lambda t \cos \Omega t, \quad (7)$$

and

$$q_2 = -a \sin \Lambda t \sin \Omega t. \quad (8)$$

The solutions represent a *resonance*: at $t = 0$, all the vibration energy is concentrated on q_1 . Then, the energy gradually moves to q_2 . At time $t = \pi/\Lambda$, all vibration energy has moved to q_2 . Then the process is reversed: the energy starts to move back to q_1 , and so on; see figure 2.

By making a coordinate transformation,

$$q'_1 = \frac{1}{\sqrt{2}}(q_1 + q_2), \quad q'_2 = \frac{1}{\sqrt{2}}(q_1 - q_2). \quad (9)$$

Heisenberg’s Hamiltonian becomes

$$H = \frac{1}{2m} p_1^2 + \frac{m}{2} \omega_1^2 q_1^2 + \frac{1}{2m} p_2^2 + \frac{m}{2} \omega_2^2 q_2^2; \quad (10)$$

with

$$\omega_1^2 = \omega^2 - 2\omega\lambda, \quad \omega_2^2 = \omega^2 + 2\omega\lambda. \quad (11)$$

Clearly, the oscillation frequency is split into two: for the first one, with a symmetric or *gerade* linear combination of coordinates, the frequency is lower. For the second one, with an antisymmetric or *ungerade* linear combination of coordinates, the frequency is higher.

In quantum mechanics, energy is related to frequency via the Planck equation,

$$E = \hbar\omega. \quad (12)$$

The interaction between the two oscillators, λ , makes an *energy level split*. If the interaction is small, approximately,

$$E = \hbar [\omega \pm \lambda]. \quad (13)$$

In summary, the interaction between the two unperturbed systems gives rise to a resonance, or a back-and-forth transfer of energy. In quantum mechanics, it gives rise to an energy level split, or *resonance energy* [13].

3. An analytically solvable case: the hydrogen molecule ion

There are only a handful of real problems in Nature that have analytic solutions in quantum mechanics, such as the hydrogen atom in Dirac theory. Those problems are essential for the understanding of the physics, and serve as the test ground for approximations. A piece of good fortune is the problem of the hydrogen molecule ion H_2^+ , a prototype for the chemical bond. The coordinates are separable, and the analytic solutions have been studied extensively. In most treatises of quantum mechanics on condensed matter, the H_2^+ problem is taken as the first and the most precise model for the understanding of condensed matter, as in Pauling's classical treatise of the chemical bond [16] and Slater's *Quantum Theory of Matter* [17].

The treatment of the H_2^+ problem in connection with NC-AFM and STM has been published previously [5]. Here we present some analysis to illustrate several points in the theory of NC-AFM and STM: three types of forces, the concept of energy splitting, the accuracy of the first-order perturbation treatment, and extension to many-body cases.

The exact solution of the H_2^+ problem gives the following asymptotic expression for energy levels as a function of the proton-proton distance r :

$$E_{\pm} = \frac{me^4}{\hbar^2} \left[-\frac{9}{4} \left(\frac{\hbar^2}{me^2r} \right)^4 - \frac{15}{2} \left(\frac{\hbar^2}{me^2r} \right)^6 - \frac{213}{4} \left(\frac{\hbar^2}{me^2r} \right)^7 + \dots \right] \pm \frac{2m^2e^6r}{\hbar^4} \exp \left\{ -1 - \frac{me^2r}{\hbar^2} \right\} \times \left[1 + \frac{1}{2} \frac{\hbar^2}{me^2r} - \frac{25}{8} \left(\frac{\hbar^2}{me^2r} \right)^2 + \dots \right]. \quad (14)$$

The first term is the van der Waals force and the core-core repulsion. The second term is the resonance energy, or the energy split between the bonding orbital and the antibonding orbital, as we will explain later. The expression in the round parentheses is

$$\frac{\hbar^2}{me^2r} \cong \frac{0.0529 \text{ nm}}{r} \quad (15)$$

actually very small in the range of interest, where the nucleus-nucleus distance r is greater than 0.25 nm. Therefore, the asymptotic expression converges rapidly.

The van der Waals energy can be evaluated using perturbation theory. It would recover the first term in the first bracket of the above expression. In the following, we will concentrate on the second line of the expression, that is, the chemical bond energy.

The treatment of the chemical bond energy of the H_2^+ problem using first-order perturbation theory is published

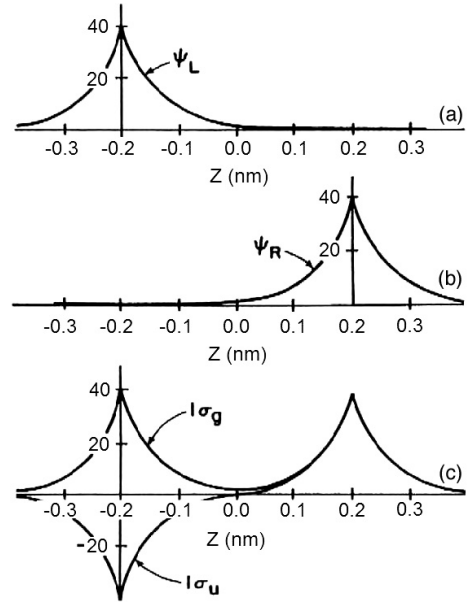


Figure 3. First-order perturbation treatment of H_2^+ .

elsewhere [5]. The basic idea is the following: starting with the ground-state wavefunctions of free hydrogen atoms, the left-hand wavefunction ψ_L and the right-hand wavefunction ψ_R , two types of combined wavefunctions can be constructed, the *gerade* or symmetric wavefunction, and the *ungerade* or antisymmetric wavefunction; see figure 3. In terms of quantum chemistry, those wavefunctions are called the bonding orbital and the antibonding orbital.

The resonance energy, or the chemical bond energy, can be evaluated using the Bardeen integral from the wavefunctions of the free atoms [5].

$$E_{\pm} \equiv \pm M = \pm \frac{\hbar^2}{2m} \int (\psi_L \nabla \psi_R - \psi_R \nabla \psi_L) dS \quad (16)$$

where the surface integral is evaluated on a medium plane between the two hydrogen atoms. It is interesting to note that the computation of chemical bond energy does not require the knowledge of the potential. Only the wavefunctions of the individual subsystems are required. This is quite similar to the resonance problem in classical mechanics, as presented in the previous section. For the hydrogen molecule ion, the result is

$$E_{\pm} = \pm \frac{2m^2e^6r}{\hbar^4} \exp \left\{ -1 - \frac{me^2r}{\hbar^2} \right\}. \quad (17)$$

To show the accuracy of the first-order perturbation treatment, the exact value of the chemical bond energy (in the solid curve), and those from perturbation theory (in the crosses) are plotted in figure 4. Over the range of operation of NC-AFM and STM, i.e., internuclear distance 0.3–0.6 nm, the difference cannot be detected by the naked eye.

The actual differences are listed in table 1. For the case of H_2^+ , we have shown that the result of first-order perturbation theory, the Bardeen integral, is quite accurate in representing the chemical bond energy over the distance range of the operation of NC-AFM and STM. In the following, we will analyse the extension to many-body cases, and its consequence in NC-AFM and STM.

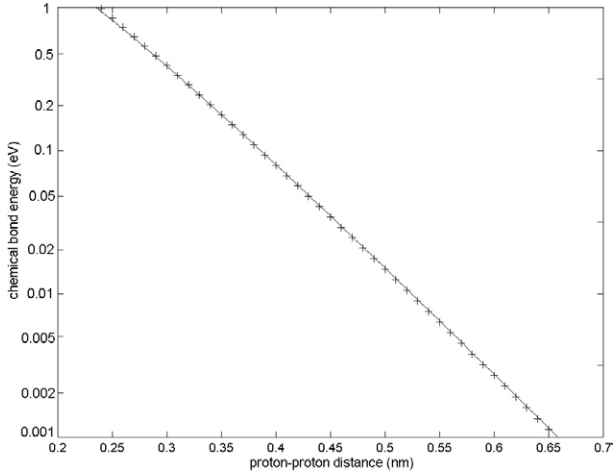


Figure 4. Accuracy of first-order perturbation treatment of H_2^+ .

Table 1. Accuracy of first-order perturbation theory in evaluating the chemical bond energy of the hydrogen molecular ion.

Internuclear distance (nm)	Chemical bond energy (eV)	Relative error	Absolute error (eV)
0.25	0.839 121	-0.034	-0.028 658
0.30	0.391 379	-0.009	-0.003 530
0.35	0.177 474	0.004	0.000 740
0.40	0.078 835	0.011	0.000 903
0.45	0.034 472	0.015	0.000 537
0.50	0.014 887	0.017	0.000 266
0.55	0.006 365	0.019	0.000 122
0.60	0.002 699	0.019	0.000 053
0.65	0.001 136	0.019	0.000 022
0.70	0.000 476	0.019	0.000 009
0.75	0.000 198	0.019	0.000 003

4. Extension to many-body cases

The case of H_2^+ is a one-body problem. To extend the treatment to many-body cases, we must take into account the statistical nature of the particles. Electrons conform to Pauli's exclusion principle, and thus Fermi-Dirac statistics. The configuration of H_2^+ actually creates four states from the ground state of a hydrogen atom: $1\sigma_g\uparrow$, $1\sigma_g\downarrow$, $1\sigma_u\uparrow$, and $1\sigma_u\downarrow$; the arrow indicates the spin state. As we have shown, the antibonding orbitals have a higher energy level. If there is one electron, then only one of the bonding orbitals is occupied. The energy level is lower than the free atoms. Thus, a chemical bond is formed. If there are two electrons, as in the case of the neutral hydrogen molecule, the two bonding orbitals with opposite spin are occupied. The total energy is again lower than that of two hydrogen atoms, and a chemical bond is formed. The case of the neutral hydrogen molecule has been worked out in detail by Gorkov and Pitaevskii [18] and also Herring and Flicker [19]. An accurate asymptotic expression for the chemical bond energy was found. This problem is very similar to the problem of H_2^+ . The difficult issue is to treat the field from another electron analytically, instead of using the self-consistent field approximation, and those authors have succeeded in handling the complicated mathematics.

The system of two He atoms has the same configuration; each has two 1s electrons, with four electrons altogether.

By bringing two He atoms together, resonance would occur. Nevertheless, all four states, $1\sigma_g\uparrow$, $1\sigma_g\downarrow$, $1\sigma_u\uparrow$, and $1\sigma_u\downarrow$, are occupied. The resonance energies of the bonding orbital and the antibonding orbital have the same value but opposite sign. The net energy change is zero. Therefore, no chemical bonds are formed. Only the van der Waals force is in effect.

In NC-AFM and STM, two pieces of solid material are brought into proximity. Resonance would take place. The bonding orbital and the antibonding orbital, similar to those in the H_2^+ problem, are formed for the combined system from the electronic states of the free systems. However, the net effect depends on the band structure. For filled bands, the situation is similar to the case of two He atoms. There is no net energy gain as a result of resonance. Only the van der Waals force exists. For completely unoccupied bands, resonance has no effect, as no electrons are present. Only for half-filled bands as in metals does resonance have an effect to lower the total energy of the combined system. In this case, only the bonding states are occupied, which have lower energy than the corresponding states of the free tip and free sample. This occurs also for metallic (half-filled) surface states on semiconductor surfaces, such as those on $Si(111)7 \times 7$.

5. An experimentally verifiable relation in NC-AFM and STM

5.1. van der Waals force

Intuitively, from the concept of resonance, there should be a relation between tunnelling and attractive atomic force, or chemical bond force. To do the experiments correctly, or more precisely speaking to do the data analysis correctly, one must bear in mind that the van der Waals force between the tip and the sample always exists. It depends on the geometry of the tip, and the material nature of the tip and the sample. It must be subtracted. Fortunately, the van der Waals force and the chemical bond force behave very differently. First, they are dominant in different distance ranges. The van der Waals force plays a dominant role at an internuclear distance greater than 0.5 nm. Second, the distance dependences are quite different. Typically, the van der Waals force varies with the inverse of the tip-sample distance, or $1/r$. The chemical force varies exponentially, with a typical decay length of 0.1 nm. Third, the van der Waals force for many practical systems is well understood. In other words, one can make a reasonable estimate of the van der Waals force under given experimental conditions.

In the following, we will make an estimate of the van der Waals force for a paraboloidal metal tip and a flat metal sample surface. Following Israelachvili [20], the van der Waals potential is

$$V = \frac{AR}{6z}, \quad (18)$$

where R is the radius of curvature of the tip, z is the distance from the tip apex to the sample surface, and A is the Hamaker constant. For metals [20],

$$A \cong (3-5) \times 10^{-19} \text{ J} \cong (2-3) \text{ eV}. \quad (19)$$

Therefore, the van der Waals potential could be as large as a good fraction of an electronvolt, and the force can be as

large as a good fraction of a nN. However, the dependence on tip-sample distance should make it easily distinguishable from the chemical bond energy.

5.2. Tunnelling current and chemical bond energy

According to the well known Fermi golden rule [5], the transition probability from a sample state ψ_v to a tip state ψ_μ is

$$w_{\mu\nu} = \frac{2\pi}{\hbar} |M_{\mu\nu}|^2 \delta(E_\mu - E_\nu), \quad (20)$$

indicating that only the states with the same energy level can have non-vanishing transition probabilities. By applying a bias V across the tunnelling junction, a tunnelling current I is generated. If the tunnelling matrix element M does not vary significantly in the energy range corresponding to the applied bias voltage V , the tunnelling current is

$$I = \frac{4\pi e}{\hbar} \int_0^{eV} \rho_S(E_F - eV + \varepsilon) \rho_T(E_F + \varepsilon) |M|^2 d\varepsilon, \quad (21)$$

where ρ_S is the sample DOS and ρ_T is the tip DOS. At small bias, both sample DOS and tip DOS can be considered as constants; the tunnelling current is

$$I = \frac{4\pi e^2}{\hbar} \rho_S \rho_T |M|^2 V. \quad (22)$$

It is worth noting that without an external bias voltage (including possible EMF generated by the thermal couple effect) there is no tunnelling current. Otherwise, a *perpetual motion* is created. Thus, the tunnelling *conductance* G is associated with the tunnelling matrix element M with a quadratic relation, regardless of the magnitude and the sign of the bias,

$$G \equiv \frac{I}{V} = \frac{4\pi^2}{R_K} \rho_S \rho_T |M|^2, \quad (23)$$

where $R_K = h/e^2 = 25\,812.8 \, \Omega$ is von Klitzing's constant.

In the following, using time-dependent perturbation theory, we will show that for metals the tunnelling matrix element in the above equation is the chemical bond energy between the states near the Fermi level on the tip and on the sample; see figure 5. Because of the condition of equal energy level, equation (20), we shall consider a pair of states in the sample and the tip with the same energy level. The argument closely resembles Heisenberg's classical mechanical illustration of quantum mechanical resonance.

In a self-consistent field picture, an electron in the combined system satisfies the following time-dependent Schrödinger equation:

$$i\hbar \frac{\partial \Psi(\mathbf{r}, t)}{\partial t} = \left[-\frac{1}{2m} \nabla^2 + U(\mathbf{r}) \right] \Psi(\mathbf{r}, t), \quad (24)$$

where $U(\mathbf{r})$ is the potential of the combined system. By considering the tip and the sample separately, we have the Schrödinger equations for the tip wavefunction,

$$i\hbar \frac{\partial \Psi_S(\mathbf{r}, t)}{\partial t} = \left[-\frac{1}{2m} \nabla^2 + U_S(\mathbf{r}) \right] \Psi_S(\mathbf{r}, t), \quad (25)$$

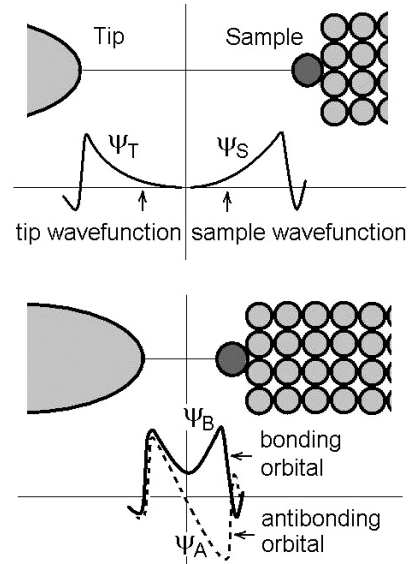


Figure 5. Perturbation treatment of the chemical bond force between a metal tip and a metal sample.

and the Schrödinger equations for the tip wavefunction,

$$i\hbar \frac{\partial \Psi_T(\mathbf{r}, t)}{\partial t} = \left[-\frac{1}{2m} \nabla^2 + U_T(\mathbf{r}) \right] \Psi_T(\mathbf{r}, t). \quad (26)$$

On the tip side, $U_S(\mathbf{r}) = 0$, and $U_T(\mathbf{r}) = U(\mathbf{r})$; on the sample side, $U_T(\mathbf{r}) = 0$, and $U_S(\mathbf{r}) = U(\mathbf{r})$; see figure 5. For the individual systems, we have solutions at the energy level E ,

$$\Psi_S(\mathbf{r}, t) = \psi_S(\mathbf{r}) e^{-iEt/\hbar}, \quad (27)$$

and

$$\Psi_T(\mathbf{r}, t) = \psi_T(\mathbf{r}) e^{-iEt/\hbar}. \quad (28)$$

Now we look for solutions of equation (24) that are linear combinations of those individual solutions. In other words, we make the following *Ansatz*:

$$\Psi(\mathbf{r}, t) = a_S(t) \psi_S(\mathbf{r}) e^{-iEt/\hbar} + a_T(t) \psi_T(\mathbf{r}) e^{-iEt/\hbar}. \quad (29)$$

Using equation (24), following the procedure in [5], we find the following equations for the evolution of the coefficients:

$$\dot{a}_T(t) = i\hbar M a_S(t), \quad (30)$$

and

$$\dot{a}_S(t) = i\hbar M a_T(t). \quad (31)$$

The matrix element M is Bardeen's integral, evaluated from the wavefunctions of the tip and the sample, on a separation surface between the tip and the sample,

$$M = \frac{\hbar^2}{2m} \int [\psi_S \nabla \psi_T^* - \psi_T \nabla \psi_S^*] d\mathbf{S}. \quad (32)$$

The specific solutions of equation (24) now depend on the initial condition. If at $t = 0$ the electron is on the tip side, the solution is

$$\Psi_1(\mathbf{r}, t) = [\cos(Mt/\hbar) \psi_T(\mathbf{r}) + i \sin(Mt/\hbar) \psi_S(\mathbf{r})] e^{-iEt/\hbar}. \quad (33)$$

This solution describes a resonance corresponding to the classical picture in figure 2. Similarly, if at $t = 0$ the electron is on the sample side, the solution is

$$\Psi_2(\mathbf{r}, t) = [\cos(Mt/\hbar)\psi_S(\mathbf{r}) + i \sin(Mt/\hbar)\psi_T(\mathbf{r})] e^{-iEt/\hbar}. \quad (34)$$

The linear combinations of those wavefunctions are also good solutions of equation (24). In particular, by adjusting the phases of the solutions that the wavefunctions ψ_1 and ψ_2 are real and positive in the gap between the tip and the sample, we have the following two solutions, as shown in figure 5:

$$\begin{aligned} \Psi_B(\mathbf{r}, t) &= \frac{1}{\sqrt{2}} [\Psi_1(\mathbf{r}, t) + \Psi_2(\mathbf{r}, t)] \\ &= \frac{1}{\sqrt{2}} [\psi_S(\mathbf{r}) + \psi_T(\mathbf{r})] e^{-i(E+M)t/\hbar}, \end{aligned} \quad (35)$$

and

$$\begin{aligned} \Psi_A(\mathbf{r}, t) &= \frac{1}{\sqrt{2}} [\Psi_1(\mathbf{r}, t) - \Psi_2(\mathbf{r}, t)] \\ &= \frac{1}{\sqrt{2}} [\psi_S(\mathbf{r}) - \psi_T(\mathbf{r})] e^{-i(E-M)t/\hbar}. \end{aligned} \quad (36)$$

The energy levels are $E + M$ and $E - M$, respectively. Therefore, in view of quantum chemistry, the wavefunctions could be called adequately a *bonding orbital* and an *antibonding orbital*.

Notice that both E and M are positive, the states are near the Fermi level, and the bands are half-filled; only the bonding state is occupied. Therefore, for that tip state and the sample states, the total energy of the combined system is lowered by M . As already shown in equation (23), for that pair of states, the tunnelling conductance is

$$G = \frac{4\pi^2}{R_K} \rho_S \rho_T |M|^2. \quad (37)$$

By taking into account all the states on the tip and the sample near the Fermi level, the tunnelling conductance is [5]

$$G = \frac{f \rho_S \rho_T}{R_K} |\Delta E|^2. \quad (38)$$

The quantity ΔE is the net energy gain of the chemical bond, or the measurable energy lowering. The quantity f is a numerical factor of order unity, depending on the shape of the tip. If the tunnelling conductance varies exponentially with distance z , as most of the experiments on clean metal surfaces do [21],

$$G \sim e^{-2\kappa z}, \quad (39)$$

where $\kappa = \sqrt{2m\phi}/\hbar$ is the decay constant. Because force F is the negative derivative of ΔE over z , combining equations (38) and (39), we obtain an explicit relation between F and G ,

$$F \cong -\kappa \sqrt{\frac{R_K G}{\rho_S \rho_T}}, \quad (40)$$

for $f \approx 1$.

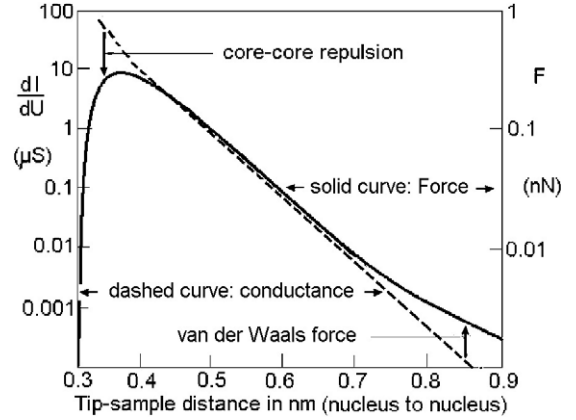


Figure 6. A graph to correlate the raw data of tunnelling conductance and the raw data of force.

5.3. Total force

By moving the tip even closer to the sample surface, the core–core repulsive force would occur. Following the idea of Morse function, the repulsive force can be represented by an omnidirectional exponential function with a decay constant twice as large as the decay constant for the attractive force, and a constant F_2 to be obtained by fitting with experimental data, for example, from the position of the equilibrium point. The total force can be written as

$$F = -\frac{AR}{6z} - F_1 e^{-\kappa z} + F_2 e^{-2\kappa z}. \quad (41)$$

Constant F_1 is related to tunnelling conductance through equation (40). If tunnelling conductance is

$$G = G_0 e^{-2\kappa z}, \quad (42)$$

then

$$F_1 \cong -\kappa \sqrt{\frac{R_K G_0}{\rho_S \rho_T}}. \quad (43)$$

This relation is central to the interpretation of combined STM and NC-AFM experiments.

5.4. Experimental verification: proposed method of data processing

STM experiments using clean metal tips and clean metal surfaces often show good exponential dependence of tunnelling conductance with tip–sample distance up to a mechanical contact [21]. Thus, the correlation between tunnelling conductance and force can be done intuitively using a graph like figure 6.

The suggested graph uses tip–sample distance as the x -axis, and the logarithms of force and tunnelling conductance as the y -axis, with a 1 by 2 scale difference. By moving one of them (tunnelling conductance or force) vertically, the two curves should match. Specifically, in the region of tunnelling with atomic resolution, for example, between $1 \mu\text{S}$ and $0.01 \mu\text{S}$, the two curves should almost overlap. The van der Waals force and the repulsive force should be separable from the chemical bond force. Parameters such as $\rho_S \rho_T$ can be extracted.

6. Threshold resistance in atom manipulation

Equation (38) should reveal itself in atom manipulation. The primary mode of atom manipulation is *pulling* [22, 23]. The mechanism of pulling can be understood from figure 5. The atom to be moved is adsorbed on the surface. In order to move it to another stable location, an activation energy E must be applied to lift the atom across the ridge of the neighbouring atoms, which is called the *diffusion barrier*. To move the atom with an STM tip, first place the tip at the top of the atom to be moved, and then apply a bias V . With the feedback loop on, gradually increase the set tunnelling current. The tip is moved towards the atom. A partial chemical bond is formed. When the chemical bond energy equals the diffusion barrier energy, the tip should be able to pull the atom over the diffusion energy barrier.

Experiments showed that the condition of pulling depends neither on the magnitude of the bias voltage, nor on its polarity. The action of pulling starts at a well defined *threshold tunnelling resistance* R . Therefore, if the chemical bond is its mechanism (rather than van der Waals or electrostatic forces), and E is the diffusion energy barrier for the adatom to overcome, from equation (38), the threshold tunnelling resistance R should be

$$R = R_K \frac{f}{\rho_S \rho_T E^2}. \quad (44)$$

Here f is a dimensionless factor of order unity, depending on the shape of the tip. Equation (44) explains the fact discovered experimentally that the threshold tunnelling resistance is independent of the magnitude *and* the polarity of the bias voltage (see figure 1(b) of [23]).

The diffusion energy barrier of individual atoms on various solid surfaces has been studied by field ion microscopy (FIM) for about half a century by the random motion of those atoms and its temperature dependence [24]. The diffusion constant can be derived from the root-mean-square value of displacement via the Einstein equation,

$$\langle (\Delta x)^2 \rangle = 2D\tau, \quad (45)$$

where D is the diffusion coefficient, τ is the time interval, and Δx is the displacement of the particle in that time interval.

Equation (1) can be rewritten in terms of number of atom jumps N within a time interval τ ,

$$\langle (\Delta x)^2 \rangle = Nl^2, \quad (46)$$

where l is the length of an elementary atomic jump. According to the Boltzmann statistics,

$$N = \tau \nu_0 \exp\left(-\frac{E_d}{kT}\right). \quad (47)$$

where ν_0 is the atomic vibration frequency, and E_d is the activation energy of surface diffusion. Therefore, from an Arrhenius plot with

$$D = \frac{\langle (\Delta x)^2 \rangle}{2\tau} \quad \text{versus} \quad \frac{1}{T}, \quad (48)$$

the activation energy E_d can be obtained. An example is shown in figure 7; see [25].

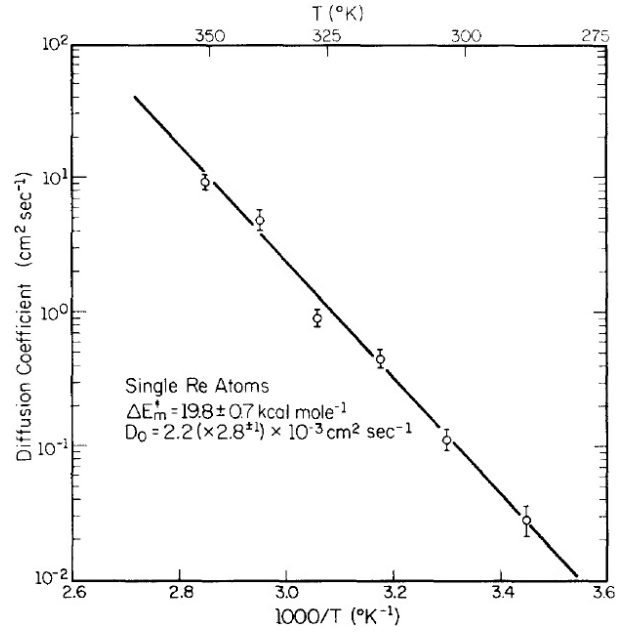


Figure 7. Extracting the value of diffusion activation energy from random-walk experiments using field-ion microscopy with an Arrhenius plot; see [25].

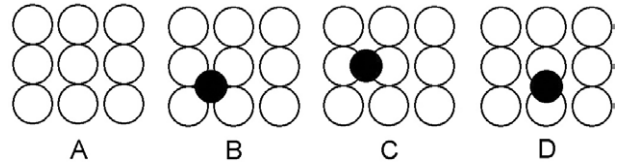


Figure 8. A suggested method for computing the activation energy using first-principle methods, for example based on density-functional theory.

The activation energy can also be computed using first-principle methods, for example, based on density-functional theory, similar to the computation in [26]. Figure 8 shows a possible computation procedure. A is a bare surface, with two different channels of diffusion. B is a configuration with an adatom at its stable site. C shows an intermediate site in the middle of the 'easy' path of diffusion. The activation energy of such a path can be obtained by computing the total energy of the ground states for configurations B and C, with the adatom staying at the prefixed x - y position, but allowing its z -position and the positions of the surrounding atoms to relax, then the energy difference of configurations B and C is the activation energy along the 'easy' path. D is the same as C, for calculating the activation energy through the 'hard' path. Actually, the computation here is simpler than that in [26].

Because E , ρ_S , and ρ_T can be derived from independent experiments (e.g., surface diffusion) or first-principle computations, following equation (44), the threshold tunnelling resistance can be *estimated or predicted quantitatively*.

Acknowledgments

The author wishes to thank Hamburg University and the DFG (Graduate School Programme) for financial support. Inspiring discussions with Professor Roland Wiesendanger, Karl-Heinz

Rieder, Alex Schwarz, Stephan Heinze, Alex Baratoff, and Ruben Perez are also appreciated.

References

- [1] Giessibl F J 1995 *Science* **260** 1451
- [2] Perez R, Stich I, Payne K and Terakura K 1997 *Phys. Rev. Lett.* **78** 678
- [3] Baratoff A 1984 *Physica B* **127** 143
- [4] Ohnishi H and Tsukada M 1989 *Solid State Commun.* **71** 391
- [5] Chen C J 1993 *Introduction to Scanning Tunneling Microscopy* (Oxford: Oxford University Press)
- [6] Ness H and Gautier F 1995 *J. Phys.: Condens. Matter* **7** 6625
- [7] Lamare L, Aourag H and Dufour J-P 1999 *J. Phys. Chem. Solids* **60** 681
- [8] Hofer W A, Redinger J and Varge P 2000 *Solid State Commun.* **113** 245
- [9] Hofer W A, Redinger J and Podloucky R 2001 *Phys. Rev. B* **64** 125108
- [10] Briner B G, Hoffmann Ph, Doering M, Rust H-P, Plummer E W and Bradshaw A M 1998 *Phys. Rev. B* **58** 13931
- [11] Heinze S, Blügel S, Pascal R, Bode M and Wiesendanger R 1998 *Phys. Rev. B* **58** 16432
- [12] Landau L D and Lifshitz E M 1977 *Quantum Mechanics (Non-Relativistic Theory)* pp 314–6
- [13] Herring C 1962 *Rev. Mod. Phys.* **34** 631
- [14] Bardeen J 1960 *Phys. Rev. Lett.* **6** 57
- [15] Heisenberg W 1926 *Z. Phys.* **38** 411
- [16] Pauling L 1948 *The Nature of the Chemical Bond* 2nd edn (Ithaca, NY: Cornell University Press) pp 8–19
- [17] Slater J C 1953 *Quantum Theory of Matter* (New York: McGraw-Hill) pp 200–13
- [18] Gorkov L P and Pitaevskii L P 1964 *Sov. Phys.—Dokl.* **8** 788
- [19] Herring C and Flicker M 1964 *Phys. Rev.* **34** A362
- [20] Israelachvili J N 1991 *Intermolecular and Surface Forces* (New York: Academic)
- [21] Schirmeisen A, Cross G, Stalder A, Grütter P and Dürig U 2000 *New J. Phys.* **2** 29
- [22] Bartels L, Meyer G and Rieder K-H 1997 *Phys. Rev. Lett.* **79** 697
- [23] Hla S-W, Braun K-F and Rieder K-H 2003 *Phys. Rev. B* **67** 201402R
- [24] Ehrlich G 1982 *CRC Crit. Rev. Solid State Mater. Sci.* **10** 391
- [25] Stolt K, Graham W R and Ehrlich G 1976 *J. Chem. Phys.* **65** 3206
- [26] Pentcheva R and Scheffler M 2002 *Phys. Rev. B* **65** 155418